THEORETICAL PHYSICS

Original article
DOI: https://doi.org/10.18721/JPM.18213

COLLECTIVE EXCITATIONS IN THE BULK DOPED SEMICONDUCTOR CADMIUM SULFIDE NANOCRYSTALS

A. N. Ipatov[1,2], *G. A. Kupriianov*[1]✉

[1] Peter the Great St. Petersburg Polytechnic University, St. Petersburg, Russia;

[2] Alferov University of RAS, St. Petersburg, Russia

✉ henryweis3@gmail.com

Abstract. The excited states of nanosized CdS semiconductor crystals with bulk doping have been studied. It was demonstrated that the giant dipole resonance dominated in their photoabsorption spectra. Varying the potential barrier height at the nanoparticle boundary was shown to be able to cause a change in the character of the collective mode from the plasmonic-type electron density fluctuations to the dimensional quantization mode depending on the particle size and the number of free charge carriers.

Keywords: semiconductor nanocrystal, cadmium sulfide, doping, plasmon resonance, multiparticle excitation

Citation: Ipatov A. N., Kupriianov G. A., Collective excitations in the bulk doped semiconductor cadmium sulfide nanocrystals, St. Petersburg State Polytechnical University Journal. Physics and Mathematics. 18 (2) (2025) 144–161. DOI: https://doi.org/10.18721/JPM.18213

Научная статья
УДК 538.9
DOI: https://doi.org/10.18721/JPM.18213

КОЛЛЕКТИВНЫЕ ВОЗБУЖДЕНИЯ В ОБЪЕМНО-ЛЕГИРОВАННЫХ ПОЛУПРОВОДНИКОВЫХ НАНОКРИСТАЛЛАХ СУЛЬФИДА КАДМИЯ

А. Н. Ипатов[1,2], *Г. А. Куприянов*[1]✉

[1] Санкт-Петербургский политехнический университет Петра Великого, Санкт-Петербург, Россия;

[2] Академический университет имени Ж. И. Алфёрова РАН, Санкт-Петербург, Россия

✉ henryweis3@gmail.com

Аннотация. Исследованы возбужденные состояния наноразмерных полупроводниковых кристаллов CdS с объемным типом легирования. Продемонстрировано, что в их спектрах фотопоглощения доминирует гигантский дипольный резонанс. Показано, что варьирование высоты потенциального барьера на границах наночастиц может приводить к изменению характера коллективной моды от колебаний электронной плотности плазмонного типа к режиму размерного квантования, в зависимости от размера частицы и числа свободных носителей заряда.

Ключевые слова: полупроводниковый нанокристалл, сульфид кадмия, легирование, плазмонный резонанс, многочастичное возбуждение

Ссылка для цитирования: Ипатов А. Н., Куприянов Г. А. Коллективные возбуждения в объемно-легированных полупроводниковых нанокристаллах сульфида кадмия // Научно-технические ведомости СПбГПУ. Физико-математические науки. 2025. Т. 18. № 2. С. 144–161. DOI: https://doi.org/10.18721/JPM.18213

Introduction

The advances in nanoelectronics in recent decades have led to an interest in creating fundamentally new materials, whose properties differ from those of the corresponding bulk components. A burgeoning field is quantum plasmonics, which includes the study of interaction between electromagnetic radiation with matter at the nanoscale [1–7]. Doped semiconductor nanocrystals show promise in this field [4, 8–13].

A characteristic feature of such nanoscale systems is the presence of dipole resonances in their optical spectra. The position of the resonance line in the spectra of semiconductor nanoparticles depends on a number of parameters, in particular, on carrier density, properties of the medium and doping type, which can be generally defined as surface or bulk [8, 14–17]. In the first case, free carriers are injected into the bulk of the semiconductor nanoparticle by donors located on its surface [18, 19], and in the second case, the charge density of free carriers is distributed over the entire bulk of the crystal and is neutralized by the dopant charge [8, 10, 14, 17]. The difference in doping methods produces a significant difference in the behavior of the dipole resonance mode excited in semiconductor nanoparticles.

As shown in [20–22], the specifics of the electronic configuration of nanocrystals with surface doping [18, 19] is that only angular degrees of freedom are excited in the collective dipole mode upon interaction with an external electromagnetic field, while the electron motion in the radial direction does not occur and the electrons oscillate tangentially relative to the boundary of the system inside a relatively thin spherical layer.

In the case of bulk-doped semiconductor nanoparticles [12, 15–17], the dipole plasmon can be described in the adiabatic approximation [23, 24] by a model of harmonic oscillations of an entire system of delocalized electrons relative to the center of the positively charged core, in the direction normal to its surface.

It was found in [20, 21] that due to the peculiarities of the electronic structure of surface-doped nanocrystals, the frequencies and oscillator strengths of their plasmon modes are almost completely determined by the contribution of correlated excitations from a single dipole transition between single-particle HOMO and LUMO levels, which made it possible to describe the optical properties of such systems within a simple two-level model [21, 25].

The situation is different for bulk doping. Evidently, for theoretical description of the collective excited state, it is necessary to take into account the contributions of at least two single-particle channels connected by correlation interaction. On the other hand, the interaction of the harmonic mode with the surface of the nanocrystal in the presence of a potential barrier between the semiconductor particle and its dielectric medium leads to splitting of the resonance line into several separate modes [25].

The optical characteristics of nanoscale semiconductor crystals with various types of doping are considered in [17], demonstrating that the spectra of dipole excitations in such systems show a transition from size quantization with a small number of free carriers to plasmon oscillations with an increased number of free charge carriers. Additionally, it is also established in [25] that regardless of the doping approach used, the optical spectrum of nanoparticles is dominated by the resonant dipole mode whose nature depends both on the dimensions of the system itself and by the type of doping and its degree, i.e., the number of delocalized charge carriers. In this case, the transition from the size quantization mode to classical plasmon oscillations of the electronic system occurs both as the number of electrons increases and as the geometric dimensions of the system increase. The very nature of plasmon oscillations, depending on the degrees of freedom involved, can vary from the translational type, where the electron cloud moves in the direction normal to the surface of the system, to the collective rotational mode, where only angular degrees of freedom are excited, while motion in the radial direction practically does not occur.

The goal of this study is to investigate the dependence of many-particle excited states in the electronic system of bulk-doped semiconductor nanocrystals on the height of the potential barrier at the boundary and on the geometric dimensions of the system, considering the example of cadmium sulfide (CdS) crystals.

Our approach is based on a self-consistent quantum mechanical description of many-particle excitations in a system of delocalized charge carriers.

Calculations of the ground state of the system were carried out in the local density approximation (LDA) taking into account the local interparticle exchange interaction by numerically solving the self-consistent Kohn–Sham equations [26].

The photoabsorption spectra of nanocrystals of various dimensions were obtained using the random phase approximation (RPA) with local exchange interaction (RPAX) [27, 28]. The system of atomic units $|e| = \hbar = m_e = 1$ is used in the study.

Theoretical approach

We consider *n*-doped CdS nanocrystals with bulk-type doping in a dielectric medium. Let us consider an electrically neutral system of fermions coupled by the Coulomb interaction. We define negative particles as electrons with an effective mass in the conduction band m^*_e. In the case considered in this paper, the full Hamiltonian $\hat{H}$ is the operator of the total energy of a system of N electrons interacting with each other via the Coulomb potential V in an external field with the potential $U_{ext}(\mathbf{r})$:

$$\hat{H} = \sum_i^N \frac{\hat{\mathbf{p}}_i^2}{2m_e^*} + \sum_i^N U_{ext}(\mathbf{r}_i) + \frac{1}{2}\sum_{i,j}^N V(\mathbf{r}_i, \mathbf{r}'_j). \tag{1}$$

The motion of delocalized electrons within the bulk of the nanoparticle is restricted by the boundary of the conduction band near the surface. The external potential $U_{ext}(\mathbf{r})$ restricting the motion of delocalized electrons is described as a spherically symmetric potential well whose geometric parameter R is determined by the given dimensions of the nanocrystal, while the positive charge under bulk doping is assumed to be evenly distributed throughout the entire volume of the system. Thus, the external potential generated by this charge within the framework of the model used takes the form of the potential of a uniformly charged sphere with the charge $Z = Ne$ in a dielectric medium [17, 25]:

$$U_{ext}(r) = \begin{cases} \dfrac{Ne^2}{2\varepsilon_1 R^3}\left(r^2 - \left(1 + \dfrac{2\varepsilon_1}{\varepsilon_2}\right)R^2\right), & 0 < r < R, \\ -\dfrac{Ne^2}{\varepsilon_2 r} + U, & r > R, \end{cases} \tag{2}$$

where U is the phenomenological parameter characterizing the height of the potential barrier at the interface between the nanocrystal and the dielectric medium (this height is commensurate in order of magnitude with the electron work function from the bulk material of the semiconductor); ε_1, ε_2 are the dielectric constants of the CdS nanocrystal and its dielectric medium, respectively; e is the elementary charge.

The Coulomb pair interaction between electrons at points $\mathbf{r}_a$ and $\mathbf{r}_b$ is screened as a result of polarization of both the semiconductor material itself (indicated by the subscript 1) and the medium (subscript 2), so that multipole decomposition of the interparticle interaction potential at $r_i, r_j < R$ can be written as follows:

$$V(\mathbf{r}_i, \mathbf{r}_j) = \sum_{LM} \frac{V_L}{2L+1} Y_{LM}(\mathbf{n}_i) Y^*_{LM}(\mathbf{n}_j),$$
$$V_L = \frac{4\pi e^2}{\varepsilon_1}\left(\frac{r_<^L}{r_>^{L+1}} + \frac{(\varepsilon_1 - \varepsilon_2)(L+1)(r_i r_j)^L}{(L\varepsilon_1 + (L+1)\varepsilon_2)R^{2L+1}}\right), \tag{3}$$

where $r_{>,<}$ are, respectively, the largest and smallest of the radii $r_{i,j}$; $Y_{LM}(\mathbf{n}_{i,j})$ are the spherical components of the electron wave function whose position in space is determined by the position vectors $\mathbf{r}_i$ and $\mathbf{r}_j$, respectively; L is the total orbital moment of the system.

The interparticle interaction in the ground state of the system is described using the Local Density Approximation (LDA) where the single-particle wave functions of electrons $\phi_i(\mathbf{r}_i)$ satisfy the self-consistent Kohn–Sham equations [26]:

$$-\frac{\hbar^2\Delta_i}{2m_e^*}\phi_i(\mathbf{r}_i)+\left(U_{ext}(\mathbf{r}_i)+U_H(\mathbf{r}_i)+U_x(\mathbf{r}_i)\right)\phi_i(\mathbf{r}_i)=E_i\phi_i(\mathbf{r}_i), \tag{4}$$

where E_i are the single-particle electron energies; $U_{\mathrm{H}}(\mathbf{r})$ is the corresponding Hartree potential; $U_x(\mathbf{r})$ is the local exchange potential.

In the case of the system with filled shells, the Hartree potential is written as

$$U_H(\mathbf{r})=\int V\left(\mathbf{r},\mathbf{r}'\right)\rho_e(\mathbf{r}')d\mathbf{r}', \tag{5}$$

where the bulk density of electrons $\rho_e(\mathbf{r})$ is calculated by summation over all filled single-particle states:

$$\rho_e(\mathbf{r})=2\sum\nolimits_i\phi_i^*(\mathbf{r})\phi_i(\mathbf{r}).$$

The local exchange potentials in the Dirac–Slater approximation $U_x(\mathbf{r})$ were defined as

$$U_x(\mathbf{r})=-\left(e^2/\varepsilon_1\right)\left(3\rho_e(\mathbf{r})/\pi\right)^{1/3}. \tag{6}$$

For spherically symmetric systems with closed electron shells and isotropic angular dependences r(**r**) and $U(\mathbf{r})$, the cumulative index i denotes

$$i=(n,\,l,\,m,\,\sigma),$$

where n is the radial quantum number; l, m are the angular momentum and its projection; σ is the spin projection.

Single-particle wave functions for such systems are written as the product of radial, angular, and spin components [29]:

$$\phi_{nlm\sigma}(\mathbf{r})=\frac{P_{nl}(r)}{r}Y_{lm}\left(\theta,\varphi\right)\chi_\sigma. \tag{7}$$

RPAX was used to describe many-electron correlations.

In this approach, the wave function of the excited state $\left|\Phi_k\right\rangle$ is represented as a superposition of single-particle excitations of the particle–vacancy type [28]:

$$\left|\Phi_k\right\rangle=\sum_{im}\left(X_{im}^{(k)}\hat{a}_m^+\hat{a}_i+Y_{im}^{(k)}\hat{a}_i^+\hat{a}_m\right)\left|\Phi_0\right\rangle, \tag{8}$$

where $\left|\Phi_0\right\rangle$ is the ground state of the system; $\hat{a}^+$, $\hat{a}$ are single-particle creation and annihilation operators; $X_{im}^{(k)}$, $Y_{im}^{(k)}$ are the amplitude coefficients for forward-in-time and backward-in-time amplitudes, respectively (characterizing the contribution of the corresponding particle–vacancy pair to the many-particle excited state $\left|\Phi_k\right\rangle$); the subscripts i, m here and below to denote filled and unfilled single-particle states of the electronic subsystem.

The excited states of the many-particle system with filled shells possessing spherical symmetry are characterized in the spin-orbit (LS) coupling approximation by the total angular momentum L and its projection M, therefore, all single-particle particle–vacancy excitations in superposition (8) have the same multipole. To describe the optical properties of the systems considered, it is sufficient to consider only dipole transitions from the ground state $\left|\Phi_0\right\rangle$ to excited multiparticle states $\left|\Phi_k\right\rangle$ with $L=1$, $M=0$.

The amplitude coefficients $\mathbf{X}^{(k)}$ and $\mathbf{Y}^{(k)}$ in superposition (8) are determined by solving the matrix equation of RPAX:

$$\mathbf{U}\mathbf{Z}^{(k)} = \hbar\Omega_k \mathbf{Z}^{(k)}, \tag{9}$$

where Ω_k are the eigenvalues of the matrix $\mathbf{U}$:

$$\mathbf{U} = \begin{pmatrix} \mathbf{A} & \mathbf{B} \\ -\mathbf{B}^* & -\mathbf{A}^* \end{pmatrix}, \quad \mathbf{Z}^{(k)} = \begin{pmatrix} \mathbf{X}^{(k)} \\ \mathbf{Y}^{(k)} \end{pmatrix}. \tag{10}$$

The elements of Hermitian matrices $\mathbf{A}$, $\mathbf{B}$ are expressed in terms of single-particle energies E_i and Coulomb matrix elements of interparticle pair interaction taking the form

$$\langle \alpha\beta | V | \gamma\eta \rangle = \delta_{\sigma_\alpha \sigma_\gamma} \delta_{\sigma_\beta \sigma_\eta} \int \phi_\alpha^*(\mathbf{r}) \phi_\beta^*(\mathbf{r}') V(\mathbf{r}, \mathbf{r}') \phi_\gamma(\mathbf{r}) \phi_\eta(\mathbf{r}') d\mathbf{r} d\mathbf{r}' \tag{11}$$

with single-particle functions obtained by solving Eqs. (4), where the potential $V(\mathbf{r},\mathbf{r}')$ is determined from expression (3).

Matrices $\mathbf{A}$ and $\mathbf{B}$ relate the single-particle excitations within the electron system:

$$\begin{aligned} A_{im,jn} &= \delta_{ij}\delta_{mn}\omega_{in} + \langle in | U | mj \rangle, \\ B_{im,jn} &= \langle ij | U | mn \rangle, \end{aligned} \tag{12}$$

where $\omega_{im} = E_m - E_i$, including both direct (Hartree) and local exchange interactions within RPAX:

$$\langle \alpha\beta | U | \gamma\eta \rangle = 2\langle \alpha\beta | V | \gamma\eta \rangle + \langle \alpha\beta | V_x | \gamma\eta \rangle, \tag{13}$$

where

$$V_x(\mathbf{r}, \mathbf{r}') = \frac{\delta U_x[\rho(\mathbf{r})]}{\delta\rho(\mathbf{r})} \delta(\mathbf{r} - \mathbf{r}'), \tag{14}$$

while the local exchange potential U_x is determined in accordance with expression (6).

The positive eigenvalues Ω_k are the transition energies between the ground state $|\Phi_0\rangle$ and the correlated excited states $|\Phi_k\rangle$ (8). The energy spectra of excited states obtained by solving Eqs. (9) and (10) and the corresponding wave functions allow to describe the processes associated with excitation of the system by various external perturbations. In particular, the response of the system to an external electromagnetic field is determined by the spectrum of dipole excitations. The oscillator strengths f_k for dipole transitions between the ground and the kth excited state are described by the formula

$$f_k = 2m_m^* D_k^2 \Omega_k, \tag{15}$$

and satisfy the Thomas–Reich–Kuhn sum rule, i.e., $\sum_k f_k = N$.

The dipole matrix elements D_k (in the length calibration) are calculated by summation over all single-particle excitations:

$$D_k = \sum_{im} \left(X_{im}^{(k)} d_{im} + Y_{im}^{(k)} d_{mi} \right), \tag{16}$$

where $d_{im} = \langle i|z|m \rangle$ are the single-particle dipole amplitudes for the particle–vacancy pair, and the amplitude coefficients $\mathbf{X}^{(k)}$ and $\mathbf{Y}^{(k)}$ are normalized by the condition

$$\sum_{im}\left(\left|X_{im}^{(k)}\right|^2-\left|Y_{im}^{(k)}\right|^2\right)=1. \qquad (17)$$

Results and discussion

This section discusses the calculation results for dipole excitation spectra of spherically symmetric bulk-doped nanoscale CdS quantum dots containing 8 delocalized electrons, forming two closed shells with the configuration $1s^2 2p^6$ in the ground state in the central field approximation, characteristic for such systems. Such a simple system was chosen as an example for illustrating the main factors associated with the influence of the potential barrier at its boundary on the spectral characteristics of the nanoparticle, aiming to minimize the number of independent parameters in the model used. Calculations were performed for different radii R of the nanocrystal and potential barrier heights U at its boundary.

Fig. 1 shows the distributions of oscillator strengths calculated by Eqs. (9) and (16), or (which is the equivalent for the local exchange potential) by Eqs. (A9) and (A18) (see Appendix It can be seen from the graphs for radii $R = 1$ and 6 nm that spectrum in the limit of 'free' systems (at $U = 0$) for both values of R consists of one dominant plasmonic line containing from 90% (at $R = 1$ nm) to 100% (at $R = 6$ nm) oscillator strengths, which is typical for harmonic oscillations of electron density as a whole. It turned out that the results obtained using the complete basis of single-particle excitations (denoted as RPAX in the graph) are almost identical to the results taking into account only two ground-state transitions: $2p \rightarrow 3d$ and $2p \rightarrow 2s$ (see Eq. (A19) of Appendix) over the entire variation range of the barrier height. There is a noticeable difference between the RPAX spectra, for which each excited state is described by linear combination (8) and the line distributions of single-particle transitions. This indicates a significant contribution of many-particle correlations to the formation of dipole modes $|\Phi_k\rangle$ (see Fig. 1), which have a collective nature.

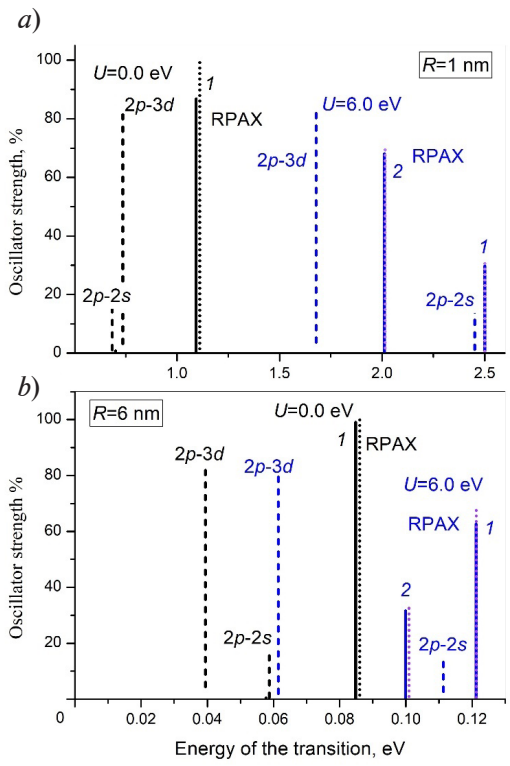

Fig. 1. Energy distribution of oscillator strengths for CdS quantum dots with $N = 8$ electrons, nanocrystal radii $R = 1$ nm (*a*) and 6 nm (*b*), at different potential barrier heights ($U = 0.0$ and 6.0 eV)

Results of exact RPAX calculation (see Eq. (9)) are shown by solid lines, results accounting for only two ground-state transitions (see Eq. (A19) in Appendix) are shown by dotted lines; oscillator strengths for these transitions are shown in single-particle approximation (dashed lines)

It was important to establish the influence of potential barrier height on the distribution of oscillator strengths in the studied spectra. We found that as this height increases, the dominant line of the collective mode splits into two distinct components and the relative distribution of oscillator strengths between them depends on the geometric dimensions of the system. Moreover, as discussed below, when a harmonic mode interacts with a potential barrier at the nanocrystal boundary, the contributions of single-particle channels $2p \rightarrow 3d$ and $2p \rightarrow 2s$ are redistributed between the two observed lines of collective modes as the potential barrier height increases. In other words, there is a significant dependence of the corresponding amplitudes $X_{im}^{(k)}$ and $Y_{im}^{(k)}$ on the height of the barrier.

As seen from Fig. 2, the distribution of electron density in the ground state of the system at different radii depends on the height of the potential barrier. This naturally leads not only to a noticeable shift of the resonant frequencies to the right as the height of the barrier increases (see Fig. 1), but also to a transformation in the radial dependence of the transition density $\rho_{tr}^{(k)}(\mathbf{r})$. The latter is defined for the kth collective mode (8) as

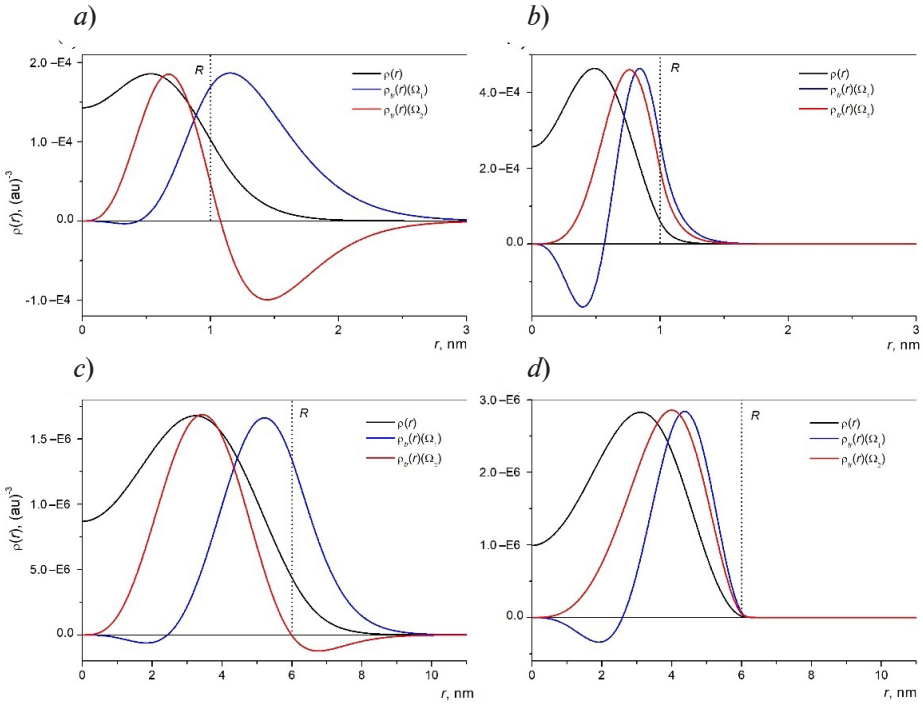

Fig. 2. Spatial distributions of electron density for ground state of CdS quantum dots with $N = 8$ electrons, nanocrystal radii $R = 1$ nm (*a, b*) and 6 nm (*c, d*), at potential barrier heights $U = 0.0$ eV (*a*, *c*) and 6.0 eV (*b*, *d*)
Radial density distributions of dipole transitions corresponding to RPAX spectral lines with frequencies Ω_1 and Ω_2 are also shown

$$\rho_{tr}^{(k)}(\mathbf{r}) = \langle \Phi_k | \delta\rho(\mathbf{r}) | \Phi_0 \rangle = \sum_{h<F, p>F} \left(X_{ph}^{(k)} \phi_p^*(\mathbf{r}) \phi_h(\mathbf{r}) + Y_{ph}^{(\nu)} \phi_p(\mathbf{r}) \phi_h^*(\mathbf{r}) \right), \quad (18)$$

where F is the Fermi level energy of the system, and $\phi(\mathbf{r})$ are single-particle wave functions (7).

In this case, there is not only a shift in the transition densities following the shift of the electron density itself to the center of the system, but also a qualitative transformation in their radial dependencies. This is most noticeable for a smaller nanocrystal (see Fig. 2, *a*, *b*). It follows therefore that a change in the barrier height causes a redistribution between the contributions of single-particle channels during the formation of the corresponding excited state (8), i.e., the ratios between the amplitudes $X^{(k)}$ and $Y^{(k)}$ change significantly. Clearly, this concerns the redistribution between the contributions of single-particle channels $2p \rightarrow 3d$ and $2p \rightarrow 2s$. Importantly, in the absence of a barrier for modes with the frequency Ω_1, the maximum transition density is observed near the interface. This is typical for surface plasmon modes where electron density fluctuations occur in the direction normal to the boundary. On the other hand, a significant part of radial density of the transitions is distributed over the bulk of the system for oscillations with the frequency Ω_2, which is typical for excited states in which rotational degrees of freedom make the main contribution [21, 22, 25].

As seen from Fig. 1, these modes are practically absent in the spectrum of excited states at $U = 0$ and the dominant line corresponds to almost 100% of the oscillator-strength sum. This indicates that electron density fluctuations in free nanoparticles exhibit the behavior of a surface plasmon harmonic mode. On the contrary, as follows from the graphs in Figs. 1 and 2, *b*, d, two dominant lines with the frequencies Ω_1 and Ω_2 are clearly observed in the presence of a potential barrier at the nanoparticle boundary in the spectrum of its dipole excitations, where almost the entire sum of the oscillator strengths is also concentrated. The maximum distribution of the transition density near the surface, characteristic for surface plasmon oscillations, is already observed for the frequency Ω_2, while a significant part of the transition density for Ω_1 falls on the internal volume of the system; this is especially pronounced for particles with smaller radii (at $R = 1$ nm).

For more detailed analysis of the influence of potential barrier on the dipole spectrum of the nanoparticles studied, we considered the dependences of oscillator strengths (8), frequencies, and amplitudes $X_{im}^{(k)}$ and $Y_{im}^{(k)}$ of collective modes, determining the contributions of individual single-particle excitations to the correlated excited state within of RPAX, on the magnitude of U at different geometric dimensions of the system. The absolute value of the backward-in-time amplitude $Y_{im}^{(k)}$ for the single-particle ground-state transition, describing the contribution of correlations in the ground state and generally comparable in order of magnitude to the corresponding forward-in-time amplitude $X_{im}^{(k)}$ for collective modes, was chosen as one of the criteria for evaluating the plasmonic behavior of the excited state considered [25, 30].

Figs. 3–6 show the results of calculations performed for nanoparticles with radii R = 1, 4, 6 and 8 nm.

Excited states in nanocrystals of radius R = 1 nm. The graphs in Fig. 3 show that the oscillator strength of the excited state oscillator with the transition frequency Ω_1 ranges from 88 to 96% of the sum rule for relatively small heights of the potential barrier U, while the contribution of the mode with the transition frequency Ω_2 remains negligible up to U = 2 eV, which is consistent with the data in Fig. 1,*a*, where a single line is observed in the RPAX spectrum. Rapid growth of the second spectral component begins above 2 eV; the oscillator strength of this component reaches the magnitude of the first one at $U \approx 3.5$ eV, after which the line with the frequency Ω_2 starts to dominate. At $U \approx 8$ eV, oscillator strengths of the two dominant modes are virtually unchanged and correlate as

$$f(\Omega_1) / f(\Omega_2) \approx 70 / 30,$$

which is typical for excitations with dominant angular and radial degrees of freedom, respectively [21, 22]. The frequencies of both dipole excitations Ω_1 и Ω_2, as well as the energy differences of single-particle levels, increase with increasing barrier height, which is observed in Fig. 1,*b*. At the same time, the oscillator strengths of single-particle transitions $2p \rightarrow 3d$ and $2p \rightarrow 2s$ remain virtually unchanged over the entire range of U values considered, suggesting that the redistribution of oscillator strengths (16) is related to the correlation interaction between these channels. This conclusion is confirmed by the behavior of the dependences of the amplitudes $X_{2p-3d}^{(k)}$ and $X_{2p-2s}^{(k)}$ for modes Ω_1 and Ω_2 (respectively) with increasing barrier height. It turned out that the main contribution to the excited state with a higher frequency Ω_1 is made primarily by the $2p \rightarrow 3d$ channel at $U \approx 0$, while the contribution of the $2p \rightarrow 2s$ channel 2 is relatively small. As the potential barrier increases, the amplitude ratio begins to change rapidly, so that correlation mixing of channels occurs, their contributions become equal at $U \approx 2.5$ eV, after which the component $2p \rightarrow 2s$ dominates.

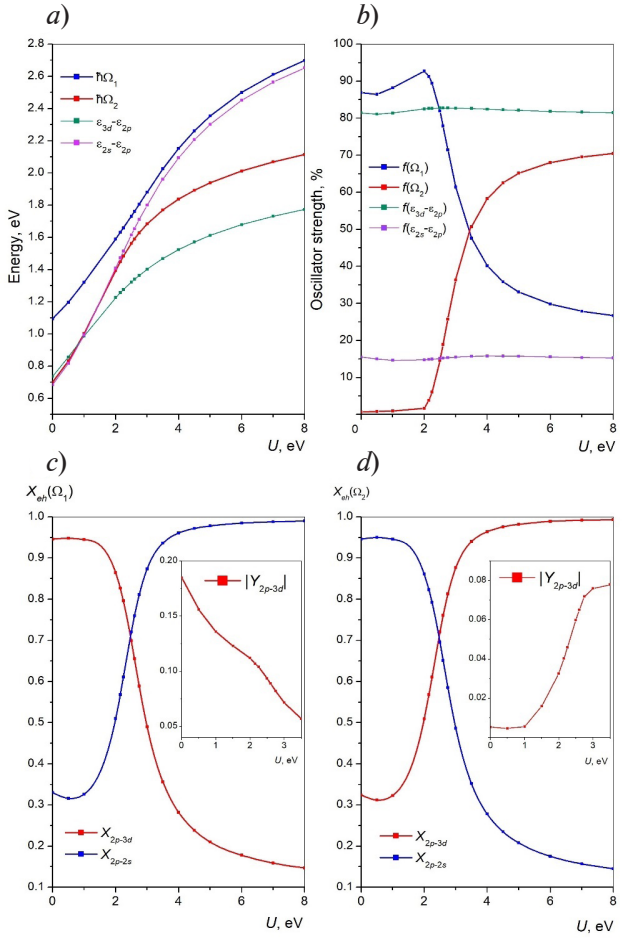

Fig. 3. Dependences of main quantities on potential barrier height U for CdS quantum dots with N = 8 electrons, radius R = 1 nm: frequencies of main collective excitations and energies of single-particle transitions (*a*); oscillator strengths (*b*); forward-in-time amplitudes X_{im} for dominant single-particle components for excited states with frequencies Ω_1 (*c*) and Ω_2 (*d*). *Insets*: dependences of backward-in-time amplitudes Y_{im} on U

The situation is reversed in the case of low-frequency excitation (with Ω_2): at first, the main contribution to the oscillator strength is made by the $2p \rightarrow 2s$ channel, but these oscillations still remain practically unexcited at $U \approx 0$, followed by rapid increase in both the oscillator strength and the amplitude of the $2p \rightarrow 3d$ component, whose contribution begins dominate at $U \geq 2.5$ eV. Ultimately, at $U \geq 4.0$ eV, it turns out that the modes are reversed with respect to the two single-particle channels dominant in sum (8) compared to the situation with a free system.

This redistribution of contributions between the main single-particle channels can be explained by the example of radial dependences of transition density (see Fig. 2). In the absence of the potential barrier, the surface plasmon-type mode is effectively excited, characterized by the distribution $\rho_{tr}(r)$ corresponding to the line with the frequency Ω_1 and the $2p \rightarrow 3d$ channel, where the radial component of the wave function $P_{3d}(r)$ has no roots in the bulk of the system. The surface plasmon behavior of this excited state is also confirmed by the relatively large absolute values of the backward-in-time amplitude $Y_{2p-3d}^{(1)} \approx 0.20-0.15$, characteristic for plasmon modes at small barrier heights, as can be seen in the inset to Fig. 3,*a*. As the barrier further increases, the excitation of electron density fluctuations in the near-surface region becomes less effective, and they are replaced by fluctuations with the dominant $2p \rightarrow 2s$ channel, where the radial component of the wave function $P_{2s}(r)$ has a root and the electron density is more uniformly distributed over the volume. The absolute value of the amplitude $Y_{2p-3d}^{(1)}$ decreases rapidly, which indicates a transition to a size-quantization mode where the electron density is localized inside a region bounded by the surface potential barrier.

Notably, the frequency Ω_1 takes values very close to the single-particle energy difference of the $2p \rightarrow 2s$ channel, while its oscillator strength tends to the corresponding single-particle value in the limit of large U (see Fig. 3, *a*, *b*). These features of frequency behavior confirm the transition of this mode from collective plasmon excitations to almost single-particle in nature.

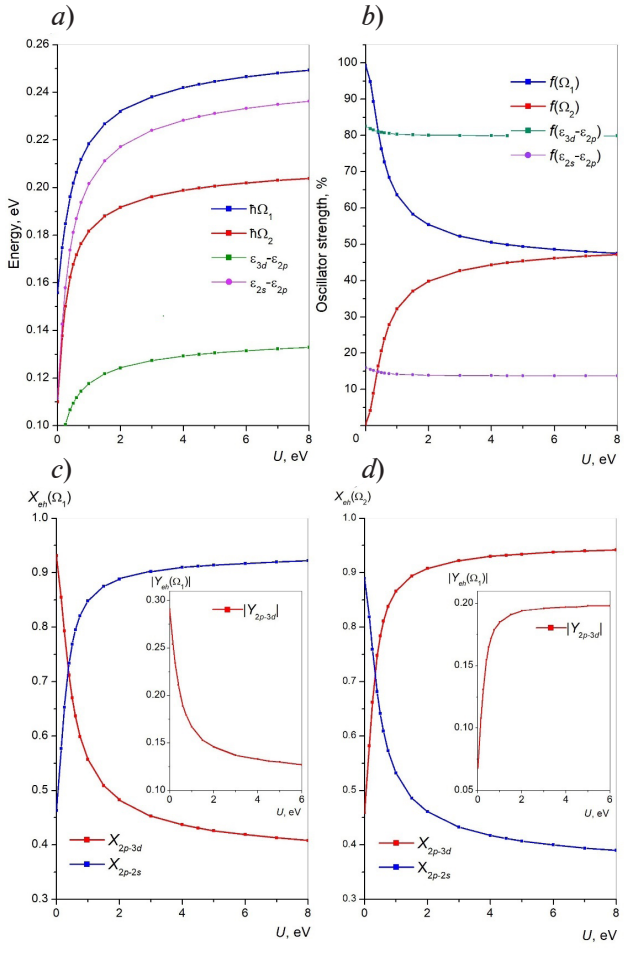

Fig. 4. Same dependences as in Fig. 3 but for nanocrystal radius $R = 4$ nm

For the second mode, where the oscillator strength begins to dominate the spectrum at $U \geq 4$ eV (see Fig. 3,*b*), its frequency Ω_2 retains, with increasing U, a noticeable difference from the energy difference of the channel $E_{3d}-E_{2p}$, which becomes the main one for this mode. This suggests that the excitation is correlated, but also localized in a potential well with the barrier U at its boundary. The absolute value of the amplitude $Y_{2p-3d}^{(2)}$ increases markedly with an increase in U although it remains smaller than 0.1. Thus, a state with the frequency Ω_2 can be described as collective excitation with dominant rotational degrees of freedom.

Excited states in nanocrystals of radius $R = 4$ nm. An increase in the radius of the system to 4 nm leads to some changes in its spectral characteristics. First, the scale of all energies decreases by an order of magnitude (see Fig. 4,*a*). At the same time, both the frequencies of collective modes and the differences of single-particle energies of the same single-particle channels $E_{2s}-E_{2p}$ and $E_{3d}-E_{2p}$, making the main contribution at $R = 1$ nm, practically cease to depend on the barrier height at $U \approx$ 4-6 eV. In other words,

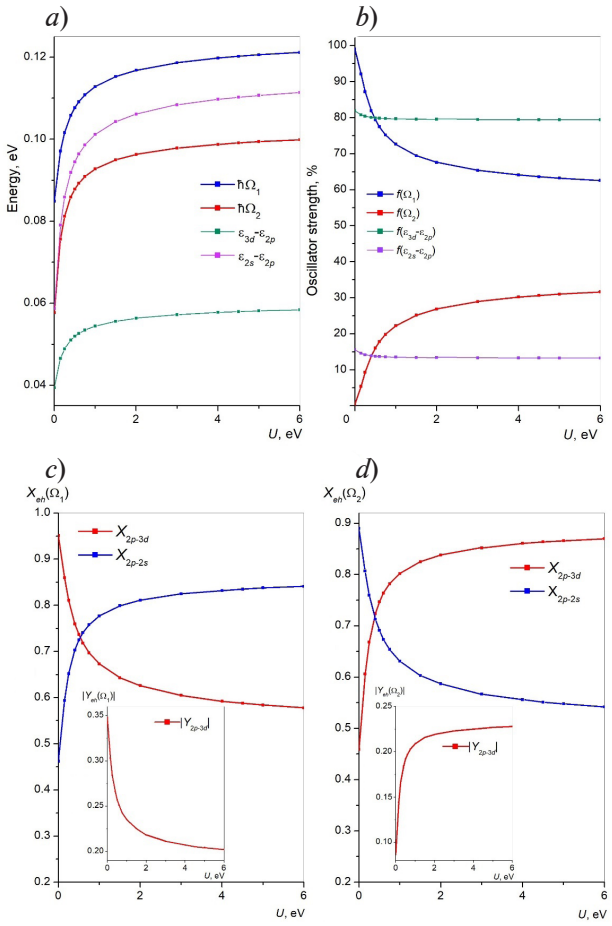

Fig. 5. Same dependences as in Figs. 3 and 4 but for nanocrystal radius $R = 6$ nm

the barrier more than an order of magnitude higher than the maximum energy of a single-particle dipole transition practically becomes infinitely high for this system. Thus, it turns out that the frequencies Ω_1 and Ω_2 of both RPAX modes differ significantly from the single-particle energy differences over the entire variation range of the barrier height, which means that interparticle correlations play a significant role in the formation of both excited states.

It can be seen from the dependence of oscillator strengths on the barrier height (Fig. 4,*b*) that the oscillator strengths of single-particle transitions remain virtually unchanged both at $R = 4$ nm and at $R = 1$ nm over the entire range of barrier heights U. As for collective modes, in the case of the free system at $U = 0$, there is also a single line with the frequency Ω_1 in the spectrum, including almost 100% of the sum rule, which is typical for excitations of the classical surface plasmon type. As in the previous case, oscillations with the frequency Ω_2 are practically not excited and their oscillator strength begins to manifest only with the appearance of the potential barrier. What is more, unlike the situation at $R = 1$ nm, the oscillator strength begins to markedly increase at small values ($U < 0.1$ eV) and upon reaching $U \approx 7-8$ eV, the oscillator strengths of both modes take a value of approximately 50% of the total value in the sum rule, becoming commensurate. Thus, for the case $R = 4$ nm, the effect of the potential barrier at $U \approx 7-8$ eV leads to the disappearance of the clearly dominant line in the dipole spectrum of the nanoparticle.

Analyzing the graphs in Fig. 4, *c*, *d* allows to draw some conclusions about the distribution of contributions of single-particle channels to correlated RPAX states (8). The same as at $R = 1$ nm, the forward-in-time amplitude of the dominant component $X^{(I)}_{2p-3d}$ exceeds 0.9 for the line with the frequency Ω_1 in the free system, but when a potential barrier appears, it decreases sharply, and the amplitude $X^{(I)}_{2p-2s}$ starts to dominate at $U \approx 0.5$ eV. In this case, the component $X^{(1)}_{2p-3d}$ does not tend to zero (as was the case at $R = 1$ nm), but retains a finite value of about 0.4, and thus the excited state turns out to be mixed based on two channels coupled by correlation interaction. The situation is reversed for the other mode with the frequency Ω_2: an increase in the barrier height leads to an increase in the contribution of the $2p \rightarrow 3d$ channel while the finite value of the amplitude $X^{(I)}_{2p-2s}$ is retained.

Let us focus more closely on the dependences for the absolute values of the backward-in-time amplitude for the more correlated $2p \rightarrow 3d$ channel (see the insets in Fig. 4, *c*, *d*). For spectral line 1, the absolute value of the amplitude $Y^{(1)}_{2p-3d}$ in the absence of potential barrier reaches about 0.3, i.e., it turns out to be of the same order as $X^{(1)}_{2p-3d}$. This makes it possible to define this mode as surface dipole plasmon with the harmonic frequency Ω_1. As the barrier height increases, both amplitudes of the $2p \rightarrow 3d$ channel begin to decrease rapidly, and mode 1 becomes close to size quantization with dominant $2p \rightarrow 2s$ component, but with significant correlations between the channels.

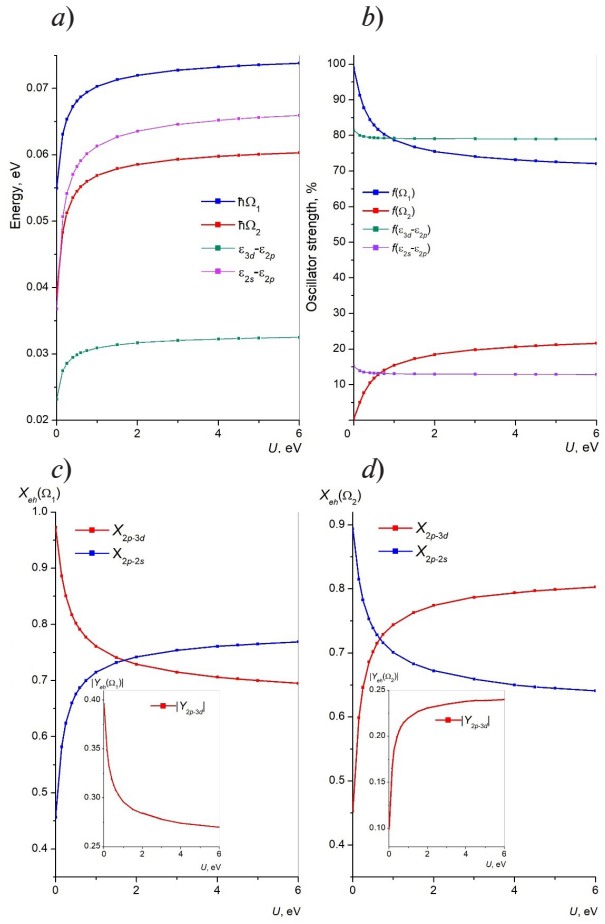

Fig. 6. Same dependences as in Figs. 3–5 but for nanocrystal radius $R = 8$ nm

The absolute value of the amplitude $Y^{(2)}_{2p-3d}$ for mode 2, whose oscillator strength increases considerably at $U \approx 2$ eV, also increases to about 0.2, and since the $2p \rightarrow 3d$ channel is the main one for this excitation at $U \geq 2$ eV, then, as with $R = 1$ nm, this mode also becomes a correlated many-particle state. The relative contributions of both excitations to the sum of oscillator strengths turn out to be equal, and thus none of the modes can be described as purely radial or purely rotational oscillations.

Excited states in nanocrystals with radii $R = 6$ and 8 nm. Calculations indicate that a further increase in the geometric dimensions of the system leads to a number of changes in the spectral characteristics of the nanocrystal under study. As the radius R of the system increases, the energy of the single-particle levels further decreases (Figs. 5,*a* and 6,*a*), but the corresponding oscillator strengths for the ground-state transitions $2p \rightarrow 3d$ and $2p \rightarrow 2s$ virtually do not change compared with the cases $R = 1$ and 4 nm (see Figs. 5,*b* and 6,*b*). The relative increase in the energy difference between excited states in RPAX, the frequencies Ω_1 and Ω_2 as well as the energy differences between single-particle levels continues, which indicates a further increase in the role of interparticle correlations in the formation of collective modes (8). As for the oscillator strengths of collective modes, the situation turns out to be different compared to the results shown in Fig. 3. As seen from Figs. 5,*b* and 6,*b*, the potential barrier appearing at the system boundary no longer leads to significant redistribution of oscillator strengths of dipole modes. Despite the appearance of the spectral line with the frequency Ω_2, the contribution of the mode with Ω_1 (as follows from the data in Figs. 5,*b* and 6,*b*) remains dominant, further gaining dominance with increasing radius R and reaching large values of U in the limit (about 75% of the total value in the sum rule) at $R = 8$ nm.

On the other hand, as in the situations discussed above, the interaction of the electron system with the potential barrier leads to redistribution of the contributions of single-particle channels to the collective excited state. The increase in the potential on the surface of the nanoparticle still causes a redistribution of amplitudes of single-particle channels $X^{(k)}_{im}$ in collective excitations. However, the contributions of the transitions $2p \rightarrow 3d$ and $2p \rightarrow 2s$ remain of the same order over most of the entire variation range of U (see Figs. 5, *c*, *d* and 6, *c*, *d*). Thus, significant interchannel correlations in both excited states ensure their many-particle nature both in the absence of the barrier and in its presence. Furthermore, it follows from the dependences for the absolute value of backward-in-time amplitudes $Y^{(k)}_{im}(U)$ shown in the insets that the ratio of the coefficients $|Y|/X$ turns out to be smaller than or approximately equal to 0.2 for all values of the barrier height U, which serves as an indicator of plasmonic nature of both collective modes.

Thus, it can be concluded for the considered system with eight delocalized electrons ($N = 8$) that the appearance of a potential barrier at its boundary at $R > 4$ nm does not lead to a transition to the size quantization for any of the modes, while electron density fluctuations retain the character of dipole surface plasmons. The same conclusion is can be drawn by analyzing the

radial dependence of transition density for the system with $R = 6$ nm (see Fig. 2,*d*), which has a maximum at the outer boundary of the electron density for both excited states in the presence of the potential barrier with the height $U = 6$ eV at the nanocrystal boundary.

Conclusion

We considered the excited states in spherical cadmium sulfide nanocrystals of various dimensions containing 8 delocalized electrons. The interparticle interaction of electrons with each other is described by the Dirac–Slater local exchange potential. To account for the correlation effects, the random phase approximation with exchange (RPAX) was used to describe the wave functions of collective excited states.

It was found for the limit of free systems in the absence of a potential barrier at the boundary that a dominant plasmon line with a frequency Ω_1 is present in the excitation spectrum. In addition, there are two ground-state transitions in the considered systems; accounting for them within RPAX yielded results virtually identical to the results obtained accounting for full basis of single-particle excitations. The dominant line turned out to be significantly correlated, i.e., it has a many-particle nature.

The appearance of a potential barrier at the nanocrystal boundary leads to an increase in the second resonant mode with the frequency Ω_2. For nanocrystals with the radius $R = 1$ nm, as the barrier height increases, the modes change places and the second mode starts to dominate. This effect disappears as the system's dimensions increase. In particular, for nanocrystals with the radius $R = 4$ nm, with sufficiently large heights of the potential barrier, there is clearly no predominant mode, while the first line continues to dominate for larger systems at any height of the barrier.

Furthermore, as the dimensions of the system increase, interparticle correlations gain a more prominent role in the formation of the dominant dipole modes.

As for the nature of the excitations, when the system's radius is less than 4 nm, a transition to size quantization occurs for the mode Ω_1 with increasing height of the potential barrier. For nanocrystals with larger radii, such a transition does not occur for any modes or at any height of the potential barrier.

To summarize, we considered the influence of potential barrier height at the boundary and the influence of the geometric dimensions of nanocrystals on the nature of excited states in CdS nanocrystals containing 8 delocalized electrons and located in a dielectric medium.

However, to validate the obtained dependences and properties of spectral characteristics for any such systems, it is necessary to study the excited states of nanocrystals containing a larger number of free carriers.

Appendix

Application of two-level model within RPAX

If we assume that matrix elements (12) are real, Eqs. (9) and (10) can generally be rewritten in matrix form

$$\begin{pmatrix} \mathbf{A} & \mathbf{B} \\ \mathbf{B} & \mathbf{A} \end{pmatrix} \begin{pmatrix} \mathbf{X}^{(k)} \\ \mathbf{Y}^{(k)} \end{pmatrix} = \Omega_k \begin{pmatrix} \mathbf{X}^{(k)} \\ -\mathbf{Y}^{(k)} \end{pmatrix}, \tag{A1}$$

and as a system of linear equations:

$$\begin{cases} \mathbf{A}\mathbf{X}^{(k)} + \mathbf{B}\mathbf{Y}^{(k)} = \Omega_k \mathbf{X}^{(k)} \\ \mathbf{B}\mathbf{X}^{(k)} + \mathbf{A}\mathbf{Y}^{(k)} = -\Omega_k \mathbf{Y}^{(k)} \end{cases}. \tag{A2}$$

After sequential addition and subtraction of Eqs. (A2), we obtain, respectively, equations of the form

$$\begin{cases} (\mathbf{A}+\mathbf{B})\left(\mathbf{X}^{(k)} + \mathbf{Y}^{(k)}\right) = \Omega_k \left(\mathbf{X}^{(k)} - \mathbf{Y}^{(k)}\right) \\ (\mathbf{A}-\mathbf{B})\left(\mathbf{X}^{(k)} - \mathbf{Y}^{(k)}\right) = \Omega_k \left(\mathbf{X}^{(k)} + \mathbf{Y}^{(k)}\right) \end{cases}. \tag{A3}$$

Expressing the difference $(\mathbf{X}^{(k)} - \mathbf{Y}^{(k)})$ on the right-hand side of the first equation in (A3) as

$$\left(\mathbf{X}^{(k)} - \mathbf{Y}^{(k)}\right) = \Omega_k \left(\mathbf{A} - \mathbf{B}\right)^{-1} \left(\mathbf{X}^{(k)} + \mathbf{Y}^{(k)}\right), \tag{A4}$$

we obtain the following equation for the vector $(\mathbf{X}^{(k)} + \mathbf{Y}^{(k)})$:

$$\left(\mathbf{A} + \mathbf{B}\right)\left(\mathbf{X}^{(k)} + \mathbf{Y}^{(k)}\right) = \Omega_k^2 \left(\mathbf{A} - \mathbf{B}\right)^{-1} \left(\mathbf{X}^{(k)} + \mathbf{Y}^{(k)}\right) \tag{A5}$$

After premultiplying and postmultiplying Eq. (A5) by the matrix $(\mathbf{A} - \mathbf{B})^{-1/2}$ and using the obvious relation

$$\left(\mathbf{A} - \mathbf{B}\right)^{1/2} \left(\mathbf{A} - \mathbf{B}\right)^{-1/2} = 1, \tag{A6}$$

Eq. (A5) can be reduced to a more symmetrical form:

$$\left(\left(\mathbf{A} - \mathbf{B}\right)^{1/2} \left(\mathbf{A} + \mathbf{B}\right)\left(\mathbf{A} - \mathbf{B}\right)^{1/2}\right)\left(\mathbf{A} - \mathbf{B}\right)^{-1/2} \left(\mathbf{X}^{(k)} + \mathbf{Y}^{(k)}\right) = \Omega_k^2 \left(\mathbf{A} - \mathbf{B}\right)^{-1/2} \left(\mathbf{X}^{(k)} + \mathbf{Y}^{(k)}\right). \tag{A7}$$

If we introduce new notations

$$\begin{aligned} \mathbf{F} &= \left(\mathbf{A} - \mathbf{B}\right)^{1/2} \left(\mathbf{A} + \mathbf{B}\right)\left(\mathbf{A} - \mathbf{B}\right)^{1/2} \\ \mathbf{Z}^{(k)} &= \left(\mathbf{A} - \mathbf{B}\right)^{-1/2} \left(\mathbf{X}^{(k)} + \mathbf{Y}^{(k)}\right) \end{aligned}, \tag{A8}$$

then the matrix equation with respect to the eigenvectors $\mathbf{Z}^{(k)}$ takes the form

$$\mathbf{F}\mathbf{Z}^{(k)} = \Omega_k^2 \mathbf{Z}^{(k)}. \tag{A9}$$

Now it remains to determine the normalization condition for $\mathbf{Z}^{(k)}$ in accordance with Eq. (17); it follows the identity

$$\left(\mathbf{X}^{(k)} + \mathbf{Y}^{(k)}\right)\left(\mathbf{X}^{(k)} - \mathbf{Y}^{(k)}\right) \equiv \sum_{im} \left(X_{im}^{(k)} + Y_{im}^{(k)}\right)\left(X_{im}^{(k)} - Y_{im}^{(k)}\right) = 1. \tag{A10}$$

It follows from Eqs. (A7) and (A3), respectively, that

$$\left(\mathbf{X}^{(k)} + \mathbf{Y}^{(k)}\right) = \left(\mathbf{A} - \mathbf{B}\right)^{1/2} \mathbf{Z}^{(k)}, \tag{A11}$$

$$\left(\mathbf{X}^{(k)} - \mathbf{Y}^{(k)}\right) = \Omega_k \left(\mathbf{A} - \mathbf{B}\right)^{-1} \left(\mathbf{X}^{(k)} + \mathbf{Y}^{(k)}\right) = \Omega_k \left(\mathbf{A} - \mathbf{B}\right)^{-1/2} \mathbf{Z}^{(k)}. \tag{A12}$$

Thus, according to equalities (A10)–(A12), normalization of the eigenvectors follows the expression

$$\sum_{im} \left(X_{im}^{(k)} + Y_{im}^{(k)}\right)\left(X_{im}^{(k)} - Y_{im}^{(k)}\right) = \Omega_k \left(\mathbf{A} - \mathbf{B}\right)^{1/2} \left(\mathbf{A} - \mathbf{B}\right)^{-1/2} \sum_{im} \left(Z_{im}^{(k)}\right)^2 = \Omega_k \sum_{im} \left(Z_{im}^{(k)}\right)^2 = 1. \tag{A13}$$

We assume that the eigenvectors obtained by solving Eq. (A9) are initially normalized in accordance with the condition $\sum_{im} \left(Z_{im}^{(k)}\right)^2 = 1$, so their elements should be subsequently renormalized to satisfy the requirement

$$\sum_{im} \left(Z_{im}^{(k)}\right)^2 = \Omega_k^{-1}. \tag{A14}$$

In turn, this transforms expression (16) for the oscillator strengths as follows:

$$D_k = \Omega_k^{-1/2} \sum_{im} d_{im} \left(\left(\mathbf{A} - \mathbf{B} \right)^{1/2} \mathbf{Z}^{(k)} \right)_{im}, \tag{A15}$$

where the elements of the vector $\mathbf{Z}^{(k)}$ are normalized by unity, i.e., $|\mathbf{Z}^{(k)}| = 1$.

Now, after considering the general case, let us examine the special one, when the interparticle exchange interaction is described in the local density approximation, for example, using local exchange potentials (6) and (14). In this case, the elements of matrices (12) turn out to be equal, namely

$$\langle in | U | mj \rangle = \langle ij | U | mn \rangle,$$

and, consequently, the following equations hold true:

$$\begin{aligned} \mathbf{A} + \mathbf{B} &= \boldsymbol{\omega} + 2\mathbf{U}, \\ \mathbf{A} - \mathbf{B} &= \boldsymbol{\omega}, \end{aligned} \tag{A16}$$

and, thus, expressions (A8) take the following form:

$$\begin{aligned} \mathbf{F} &= \boldsymbol{\omega}^{1/2} \left(\boldsymbol{\omega} + 2\mathbf{U} \right) \boldsymbol{\omega}^{1/2}, \\ \mathbf{Z}^{(k)} &= \boldsymbol{\omega}^{-1/2} \left(\mathbf{X}^{(k)} + \mathbf{Y}^{(k)} \right). \end{aligned} \tag{A17}$$

In turn, the oscillator strengths (A15) are now expressed in terms of the elements of the eigenvectors $\mathbf{Z}^{(k)}$ as

$$D_k = \Omega_k^{-1/2} \sum_{im} \omega_{im}^{1/2} d_{im} Z_{im}^{(k)}. \tag{A18}$$

Thus, applying the RPAX equation in the form (A9) taking into account expressions (A17)allows to reduce the dimension of the matrix by two times compared to the initial expression (10), but unfortunately, this makes it impossible to independently analyze the contribution of the forward-in-time and backward-in-time amplitudes to superposition (8) characterizing the many-particle excited state.

If the dominant contribution to superposition of single-particle excitations (8) is given by only two ground-state transitions, conventionally denoted by the subscripts 1 and 2, the matrix equation (A9) takes the form of a system of two linear equations:

$$\begin{cases} \left(\Omega^2 - \omega_1 \left(\omega_1 + 2U_{11} \right) \right) Z^{(1)} - 2 \left(\omega_1 \omega_2 \right)^{1/2} U_{12} Z^{(2)} = 0, \\ -2 \left(\omega_1 \omega_2 \right)^{1/2} U_{21} Z^{(1)} + \left(\Omega^2 - \omega_2 \left(\omega_2 + 2U_{22} \right) \right) Z^{(2)} = 0, \end{cases} \tag{A19}$$

where ω_1, ω_2 are the frequencies of the corresponding transitions and the condition $U_{12} = U_{21}$is satisfied for matrix elements.

The condition that the determinant of system (A19) be equal to zero implies a second-order algebraic equation with respect to the squared frequencies of collective excitations Ω^2:

$$\Omega^4 + b\Omega^2 + c = 0, \tag{A20}$$

where

$$\begin{aligned} b &= -\left(\omega_1^2 + \omega_2^2 + 2 \left(\omega_1 U_{11} + \omega_2 U_{22} \right) \right), \\ c &= \omega_1 \omega_2 \left(\left(\omega_1 + 2U_{11} \right) \left(\omega_2 + U_{22} \right) - 4U_{12}^2 \right). \end{aligned} \tag{A21}$$

It is easy to verify that in the limiting case of non-interacting particles at

$$U_{ij} = 0,\ b = -\left(\omega_1^2 + \omega_2^2\right) \text{ and } c = \omega_1^2\omega_2^2$$

we obtain the following trivial solution:

$$\Omega_{1,2} = \frac{1}{2}\left(\left(\omega_1^2 + \omega_2^2\right) \pm \sqrt{\left(\omega_1^2 + \omega_2^2\right)^2 - 4\omega_1^2\omega_2^2}\right) = \begin{cases}\omega_1 \\ \omega_2\end{cases}.$$

REFERENCES

1. **Klimov V. V.,** Nanoplasmonics, Jenny Stanford Publishing, New York, 2014.

2. **Bozhevolniy S. I.**, **Martin-Moreno L., Garcia-Vidal F.** (Eds.), Quantum plasmonics (Springer Series in Solid-State Sciences. Vol. 185), Springer International Publishing, Cham, Switzeland, 2017.

3. **Enoch S., Bonod N.,** Plasmonics: From basics to advanced topics. (Springer Series in Optical Sciences. Vol. 167), Springer-Verlag, Heidelberg, Berlin, 2012.

4. **Tame M. S., McEnery K. R., Özdemir Ş. K., et al.,** Quantum plasmonics, Nat. Phys. 9 (June) (2013) 329–340.

5. **Fedorov A. V., Rukhlenko I. D., Baranov A. V., Kruchinin S. Yu.,** Optical properties of semiconductor quantum dots, Nauka, Saint-Petersburg, 2011 (in Russian).

6. **Gusev A. I.,** Nanomaterials, nanostructures, and nanotechnologies, Fizmatlit, Moscow, 2005 (in Russian).

7. **Gaponenko S. V.,** Optical properties of semiconductor nanocrystals, Cambridge University Press, Cambridge, 1998.

8. **Routzahn A. L., White S. L., Fong L.-K., Jain P. K.,** Plasmonics with doped quantum dots, Isr. J. Chem. 52 (11–12) (2012) 983–991.

9. **Klimov V. I., Thompson B. J.,** Nanocrystal quantum dots, Second edition, CRC Press, Boca Raton, Florida, USA, 2010.

10. **Kriegel I., Scotognella F., Manna L.,** Plasmonic doped semiconductor nanocrystals: Properties, fabrication, applications and perspectives, Phys. Rep. 674 (28 Febr) (2017) 1–52.

11. **Scotognella F., Della Valle G., Kandada A. R. S., et al.,** Plasmonics in heavily-doped semiconductor nanocrystals, Eur. Phys. J. B. 86 (4) (2013) 154.

12. **Liu X., Swihart M. T.,** Heavily-doped colloidal semiconductor and metal oxide nanocrystals, an emerging new class of plasmonic nanomaterials, Chem. Soc. Rev. 43 (11) (2014) 3908–3920.

13. **El-Sayed M. A.,** Small is different: Shape-, size-, and composition-dependent properties of some colloidal semiconductor nanocrystals, Acc. Chem. Res. 37 (5) (2004) 326–333.

14. **Luther J. M., Jain P. K., Ewers T., Alivisators A. P.,** Localized surface plasmon resonances arising from free carriers in doped quantum dots, Nat. Mater. 10 (May) (2011) 361–366.

15. **Faucheaux J. A., Stanton A. L. D., Jain P. K.,** Plasmon resonances of semiconductor nanocrystals: Physical principles and new opportunities, J. Phys. Chem. Lett. 5 (6) (2014) 976–985.

16. **Lounis S. D., Runnerstrom E. L., Bergerud A., et al.,** Influence of dopant distribution on the plasmonic properties of indium tin oxide nanocrystals, J. Am. Chem. Soc. 136 (19) (2014) 7110–7116.

17. **Zhang H., Kulkarni V., Prodan E., et al.,** Theory of quantum plasmon resonances in doped semiconductor nanocrystals, J. Phys. Chem. C. 118 (29) (2014) 16035–16042.

18. **Schimpf A. M., Thakkar N., Gunthardt C. E., et al.,** Charge-tunable quantum plasmons in colloidal semiconductor nanocrystals, ACS Nano. 8 (1) (2014) 1065–1072.

19. **Schimpf A. M., Gunthardt C. E., Rinehart J. D., et al.,** Controlling carrier densities in photochemically reduced colloidal ZnO nanocrystals, J. Am. Chem. Soc. 135 (44) (2013) 16569–16577.

20. **Ipatov A. N., Gerchikov L. G., Guet C.,** Plasmon resonance in photoabsorption of colloidal highly doped ZnO nanocrystals, Nanoscale Res. Lett. 13 (1) (2018) 297.

21. **Gerchikov L. G., Ipatov A. N.,** Rotational dipole plasmon mode in nanoscale semiconductor particles, J. Exp. Theor. Phys., 132 (6) (2021) 922–940.

22. **Ipatov A. N.,** Dipole plasmon mode in nanosize semiconductor core-shell quantum dots with a type II heterojunction, J. Exp. Theor. Phys., 136 (6) (2023) 765–777.

23. **Gerchikov L. G., Guet C., Ipatov A. N.,** Multiple plasmons and anharmonic effects in small metallic clusters, Phys. Rev. A. 66 (5) (2002) 053202.

24. **Ipatov A. N., Gerchikov L. G., Guet C.,** Resonant photoabsorption of metallic clusters in a strong laser field, Comput. Mater. Sci. 35 (3) (2006) 347–353.

25. **Ipatov A. N., Kupriianov G. A.,** The plasmon resonance in the cadmium selenide semiconductor nanocrystals with different doping types, St. Petersburg State Polytechnical University J. Phys. and Math. 16 (2) (2023) 27–51 (in Russian).

26. **Dreizler R. M., Gross E. K. U.,** Density functional theory: An approach to the quantum many-body problem, Springer, Berlin, 1990.

27. **Madjet M., Guet G., Johnson W. R.,** Comparative study of exchange-correlation effects on electron and optical properties of alkali-metal clusters, Phys. Rev. A. 51 (2) (1995) 1327–1339.

28. **Mukherjee D.,** Applied many-body methods in spectroscopy and electronic structure, Springer, New York, 1992.

29. **Landau L. D., Lifshitz E. M.,** Quantum mechanics. Non-relativistic theory (Course of theoretical physics. Vol. 3), Pergamon Press, Oxford, London, New York, Paris, 1965.

30. **Bertsch G. F., Broglia R. A.,** Oscillations in finite quantum systems, Cambridge University Press, Cambridge, 1994.

СПИСОК ЛИТЕРАТУРЫ

1. **Климов В. В.** Наноплазмоника. М.: Физматлит, 2009. 480 с.

2. **Bozhevolniy S. I.**, **Martin-Moreno L., Garcia-Vidal F.** (Eds.) Quantum plasmonics. (Springer Series in Solid-State Sciences. Vol. 185). Cham, Switzeland: Springer International Publishing, 2017. 327 p.

3. **Enoch S., Bonod N.** Plasmonics: From basics to advanced topics. (Springer Series in Optical Sciences. Vol. 167). Heidelberg, Berlin: Springer-Verlag, 2012. 321 p.

4. **Tame M. S., McEnery K. R., Özdemir Ş. K., Lee J., Maier S. A., Kim M. S.** Quantum plasmonics // Nature Physics. 2013. Vol. 9. June. Pp. 329–340.

5. **Федоров А. В., Рухленко И. Д., Баранов А. В., Кручинин С. Ю.** Оптические свойства полупроводниковых квантовых точек. СПб.: Наука, 188 .2011 с.

6. **Гусев А. И.** Наноматериалы, наноструктуры, нанотехнологии. М.: Физматлит, 2005. 416 с.

7. **Gaponenko S. V.** Optical properties of semiconductor nanocrystals. Cambridge, UK: Cambridge University Press, 1998. 245 p.

8. **Routzahn A. L., White S. L., Fong L.-K., Jain P. K.** Plasmonics with doped quantum dots // Israel Journal of Chemistry. 2012. Vol. 52. No. 11–12. Pp. 983–991.

9. **Klimov V. I., Thompson B. J.** Nanocrystal quantum dots. Second edition. Boca Raton, Florida, USA: CRC Press, 2010. 485 p.

10. **Kriegel I., Scotognella F., Manna L.** Plasmonic doped semiconductor nanocrystals: Properties, fabrication, applications and perspectives // Physics Reports. 2017. Vol. 674. 28 February. Pp. 1–52.

11. **Scotognella F., Della Valle G., Kandada A. R. S., Zavelani-Rossi M., Longhi S., Lanzani G., Tassone F.** Plasmonics in heavily-doped semiconductor nanocrystals // The European Physical Journal B. 2013. Vol. 86. No. 4. P. 154.

12. **Liu X., Swihart M. T.** Heavily-doped colloidal semiconductor and metal oxide nanocrystals, an emerging new class of plasmonic nanomaterials // Chemical Society Reviews. 2014. Vol. 43. No. 11. Pp. 3908–3920.

13. **El-Sayed M. A.** Small is different: Shape-, size-, and composition-dependent properties of some colloidal semiconductor nanocrystals // Accounts of Chemical Research. 2004. Vol. 37. No. 5. Pp. 326–333.

14. **Luther J. M., Jain P. K., Ewers T., Alivisators A. P.** Localized surface plasmon resonances arising from free carriers in doped quantum dots // Nature Materials. 2011. Vol. 10. May. Pp. 361–366.

15. **Faucheaux J. A., Stanton A. L. D., Jain P. K.** Plasmon resonances of semiconductor nanocrystals: Physical principles and new opportunities // The Journal of Physical Chemistry Letters. 2014. Vol. 5. No. 6. Pp. 976–985.

16. **Lounis S. D., Runnerstrom E. L., Bergerud A., Nordlund D., Milloron D. J.** Influence of dopant distribution on the plasmonic properties of indium tin oxide nanocrystals // Journal of the American Chemical Society. 2014. Vol. 136. No. 19. Pp. 7110–7116.

17. **Zhang H., Kulkarni V., Prodan E., Nordlander P., Govorov A. O.** Theory of quantum plasmon resonances in doped semiconductor nanocrystals // The Journal of Physical Chemistry C. 2014. Vol. 118. No. 29. Pp. 16035–16042.

18. **Schimpf A. M., Thakkar N., Gunthardt C. E., Masiello D. J., Gamelin D. R.** Charge-tunable quantum plasmons in colloidal semiconductor nanocrystals // ACS Nano (The American Chemical Society). 2014. Vol. 8. No. 1. Pp. 1065–1072.

19. **Schimpf A. M., Gunthardt C. E., Rinehart J. D., Mayer J. M., Gamelin D. R.** Controlling carrier densities in photochemically reduced colloidal ZnO nanocrystals // Journal of the American Chemical Society. 2013. Vol. 135. No. 44. Pp. 16569–16577.

20. **Ipatov A. N., Gerchikov L. G., Guet C.** Plasmon resonance in photoabsorption of colloidal highly doped ZnO nanocrystals // Nanoscale Research Letters. 2018. Vol. 13. No. 1. P. 297.

21. **Герчиков Л. Г., Ипатов А. Н. В**ращательная дипольная плазмонная мода в наноразмерных полупроводниковых частицах // Журнал экспериментальной и теоретической физики. 2021. Т. 159. № 6. С. 1047–1069.

22. **Ипатов А. Н.** Дипольная плазмонная мода в наноразмерных полупроводниковых квантовых точках типа «ядро-оболочка» с гетеропереходом второго рода // Журнал экспериментальной и теоретической физики. 2023. Т. 163. № 6. С. 858–872.

23. **Gerchikov L. G., Guet C., Ipatov A. N.** Multiple plasmons and anharmonic effects in small metallic clusters // Physical Review A. 2002. Vol. 66. No. 5. P. 053202.

24. **Ipatov A. N., Gerchikov L. G., Guet C.** Resonant photoabsorption of metallic clusters in a strong laser field // Computational Materials Science. 2006. Vol. 35. No. 3. Pp. 347–353.

25. **Ипатов А. Н., Куприянов Г. А.** Плазмонный резонанс в полупроводниковых нанокристаллах селенида кадмия с различным типом легирования // Научно-технические ведомости СПбГПУ. Физико-математические науки. 2023. Т. 16. № 2. С. 27–51.

26. **Dreizler R. M., Gross E. K. U.** Density functional theory: An approach to the quantum many-body problem. Berlin: Springer, 1990. 302 p.

27. **Madjet M., Guet G., Johnson W. R.** Comparative study of exchange-correlation effects on electron and optical properties of alkali-metal clusters // Physical Review A. 1995. Vol. 51. No. 2. Pp. 1327–1339.

28. **Mukherjee D.** Applied many-body methods in spectroscopy and electronic structure. New York, USA: Springer, 1992. 299 p.

29. **Ландау Л. Д., Лифшиц Е. М.** Теоретическая физика. В 10 тт. Т. 3. Квантовая механика (нерелятивистская теория). -4е изд., испр. М.: Наука. Гл. ред. физ.-мат. лит-ры, 1989. 768 с.

30. **Bertsch G.F., Broglia R.A.** Oscillations in finite quantum systems. Cambridge, UK: Cambridge University Press, 1994. 232 p.

THE AUTHORS

IPATOV Andrei N.
Peter the Great St. Petersburg Polytechnic University,
Alferov University of RAS
29 Politechnicheskaya St., St. Petersburg, 195251, Russia
andrei_ipatov@mail.ru
ORCID: 0000-0003-1457-8236

KUPRIIANOV Genrikh A.
Peter the Great St. Petersburg Polytechnic University
29 Politechnicheskaya St., St. Petersburg, 195251, Russia
henryweis3@gmail.com
ORCID: 0009-0001-5775-2276

СВЕДЕНИЯ ОБ АВТОРАХ

ИПАТОВ Андрей Николаевич – *доктор физико-математических наук, профессор кафедры физики Санкт-Петербургского политехнического университета Петра Великого и профессор кафедры физики и технологии наногетероструктур Санкт-Петербургского академического университета имени Ж. И. Алфёрова РАН.*
195251, Россия, г. Санкт-Петербург, Политехническая ул., 29
andrei_ipatov@mail.ru
ORCID: 0000-0003-1457-8236

КУПРИЯНОВ Генрих Александрович – *ассистент кафедры физики Санкт-Петербургского политехнического университета Петра Великого.*
195251, Россия, г. Санкт-Петербург, Политехническая ул., 29
henryweis3@gmail.com
ORCID: 0009-0001-5775-2276

Received 06.05.2024. Approved after reviewing 02.12.2024. Accepted 02.12.2024.
Статья поступила в редакцию 06.05.2024. Одобрена после рецензирования 02.12.2024. Принята 02.12.2024.